

## Twin superlattice-induced large surface recombination velocity in GaAs nanostructures

Chunyang Sheng, Evan Brown, Fuyuki Shimojo, and Aiichiro Nakano

Citation: [Applied Physics Letters](#) **105**, 231602 (2014); doi: 10.1063/1.4903487

View online: <http://dx.doi.org/10.1063/1.4903487>

View Table of Contents: <http://scitation.aip.org/content/aip/journal/apl/105/23?ver=pdfcov>

Published by the [AIP Publishing](#)

---

### Articles you may be interested in

[Effects of twins on the electronic properties of GaAs](#)

Appl. Phys. Lett. **103**, 022105 (2013); 10.1063/1.4811746

[Photovoltaic effects on Franz–Keldysh oscillations in photoreflectance spectra: Application to determination of surface Fermi level and surface recombination velocity in undoped GaAs/n-type GaAs epitaxial layer structures](#)

J. Appl. Phys. **97**, 063708 (2005); 10.1063/1.1861968

[Photoluminescence study of the dynamical properties of GaAs sawtooth superlattices](#)

J. Appl. Phys. **82**, 5748 (1997); 10.1063/1.366439

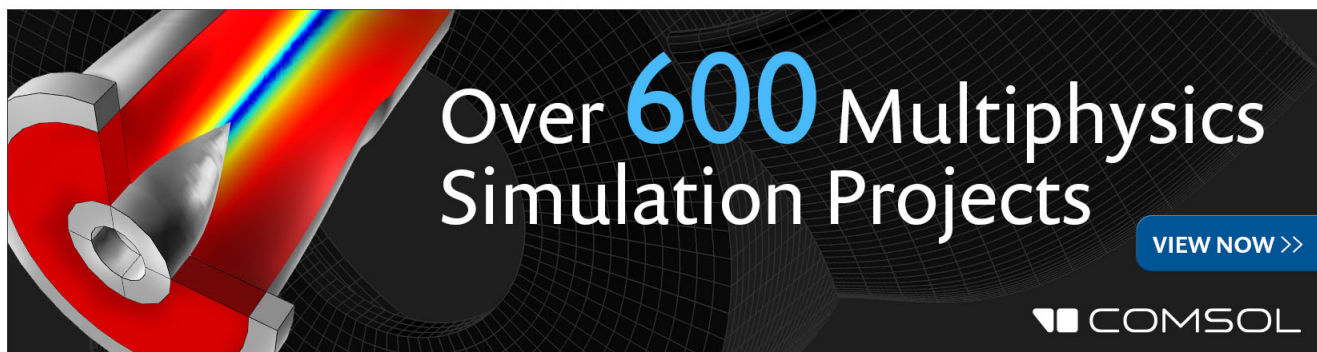
[Detection of surface states in GaAs and InP by thermally stimulated exoelectron emission spectroscopy](#)

J. Appl. Phys. **82**, 5597 (1997); 10.1063/1.366420

[Temperature dependence of photoluminescence spectra in InAs/GaAs quantum dot superlattices with large thicknesses](#)

J. Appl. Phys. **82**, 4489 (1997); 10.1063/1.366255

---

An advertisement for COMSOL Multiphysics. On the left, a 3D cutaway diagram of a mechanical part is shown with a color gradient from red to blue, representing a simulation. The background is dark with a grid pattern. The text 'Over 600 Multiphysics Simulation Projects' is written in large, white and blue font. A blue button with white text says 'VIEW NOW >>'. The COMSOL logo is in the bottom right corner.

Over **600** Multiphysics Simulation Projects

[VIEW NOW >>](#)

COMSOL

## Twin superlattice-induced large surface recombination velocity in GaAs nanostructures

Chunyang Sheng,<sup>1</sup> Evan Brown,<sup>1</sup> Fuyuki Shimojo,<sup>1,2</sup> and Aiichiro Nakano<sup>1</sup>

<sup>1</sup>*Collaboratory for Advanced Computing and Simulations, Department of Physics and Astronomy, Department of Computer Science, Department of Chemical Engineering and Materials Science, University of Southern California, Los Angeles, California 90089-0242, USA*

<sup>2</sup>*Department of Physics, Kumamoto University, Kumamoto 860-8555, Japan*

(Received 15 October 2014; accepted 23 November 2014; published online 8 December 2014)

Semiconductor nanowires (NWs) often contain a high density of twin defects that form a twin superlattice, but its effects on electronic properties are largely unknown. Here, nonadiabatic quantum molecular dynamics simulation shows unique surface electronic states at alternating (111)A and (111)B sidewall surfaces of a twinned [111]-oriented GaAs NW, which act as effective charge-recombination centers. The calculated large surface recombination velocity quantitatively explains recent experimental observations and provides microscopic understanding of the underlying surface-recombination processes. © 2014 AIP Publishing LLC.

[<http://dx.doi.org/10.1063/1.4903487>]

Nanowires (NWs) composed of semiconductors such as gallium arsenide (GaAs) have promising applications, including being used in solar cells.<sup>1–4</sup> Among many unique features, these NWs often contain a high density of twin defects that form a twin superlattice (TSL).<sup>5–7</sup> The geometry of TSLs has been studied extensively. In a [111]-oriented III–V semiconductor NW, a TSL is commonly accompanied by alternating (111)A and (111)B sidewall surfaces.<sup>5–7</sup> These TSLs greatly affect the electronic properties of NWs. For example, they surprisingly increase the radiative decay time of a bound exciton while decreasing the carrier mobility in a [111] oriented GaAs NW.<sup>8,9</sup>

The charge-recombination (CR) rate at NW sidewall surfaces is an important electronic property, which essentially controls the efficiency of GaAs-NW devices. In solar cells, for instance, a large fraction of photoexcited electron-hole pairs recombine and are lost before they can be collected as an electric current. Consequently, the power conversion efficiency of GaAs-NW solar cells remains relatively low. In fact, optical pump-terahertz probe time domain spectroscopy has shown orders-of-magnitude higher surface recombination velocity (SRV) for GaAs NWs compared with those in InAs and InP NWs.<sup>10</sup> Potential causes of the large SRV include the formation of surface oxides<sup>11</sup> and associated interfacial CR.<sup>12</sup> However, the effect of ubiquitous TSLs on SRV remains elusive. Fundamental scientific questions are: What is the effect of TSLs on surface electronic states, and how do they influence the SRV in GaAs NWs?

To answer these questions, we first perform quantum molecular dynamics (QMD) simulations<sup>13–15</sup> in which interatomic forces are computed from first-principles based density functional theory.<sup>16</sup> Here, electronic states are calculated using the projector-augmented-wave method,<sup>17,18</sup> which is an all-electron electronic-structure-calculation method within a frozen-core approximation. The generalized gradient approximation<sup>19</sup> is used for the exchange-correlation energy with nonlinear core corrections.<sup>20</sup> We apply self-interaction corrections to the energies of the

Kohn-Sham (KS) orbitals.<sup>21,22</sup> The momentum-space formalism is utilized,<sup>23</sup> where the plane-wave cutoff energies are 30 and 250 Ry for the electronic pseudo-wave functions and the pseudo-charge density, respectively. The energy is minimized with respect to the KS orbitals iteratively using a preconditioned conjugate-gradient method. Projector functions are generated for the 4s, 4p, and 4d states of Ga and As.

As explained above, TSLs in [111]-oriented III–V semiconductor NWs are commonly associated with {111} sidewall facets.<sup>5–7</sup> To simplify the geometry while retaining this key feature, we here simulate a GaAs nanosheet (NS)<sup>24,25</sup> as shown in Fig. 1(a). The *xy*-cross section (which is parallel to the (111) crystallographic plane of GaAs zinc blende crystal) of the NS has side lengths of 45.00 Å and 15.99 Å in the *x* and *y* directions, which are aligned with the [110] and [11 $\bar{2}$ ] directions, respectively. (111) GaAs bilayers are stacked in such a way as to expose Ga-terminated (111)A and As-terminated (111)B type sidewall surfaces, whereas the periodic boundary condition (PBC) is applied in the *y* direction to emulate an infinite NS. A stacking defect is inserted in the middle of the simulation box in the *z* direction to revert the stacking sequence (Fig. 1(a)). We apply the PBC in the *z* direction, and consequently there are two twin boundary planes, one at  $z = L_z/2$  and the other at  $z = L_z$  or equivalently at  $z = 0$  due to the PBC, where  $L_z = 39.17$  Å is the height of the simulation box in the *z* direction. This amounts to a TSL with a twin-twin distance of  $L_z/2 = 19.58$  Å, which is typical in experimental systems. The simulated system contains 768 atoms, and the  $\Gamma$  point is used for Brillouin zone sampling.

We first obtain the minimum-energy atomic configuration by relaxing the atomic positions using the quasi-Newton method. By doing so with ideal (111)A and (111)B sidewall surfaces, we found the configuration to be mechanically unstable, with some Ga atoms detaching from the (111)A surfaces. This is understandable in light of the relatively high surface energies of the ideal surfaces compared to some of the reconstructed surfaces.<sup>26</sup> We thus consider GaAs (111)B sidewalls with Ga-adatom reconstructions (Fig. 1(b)) and

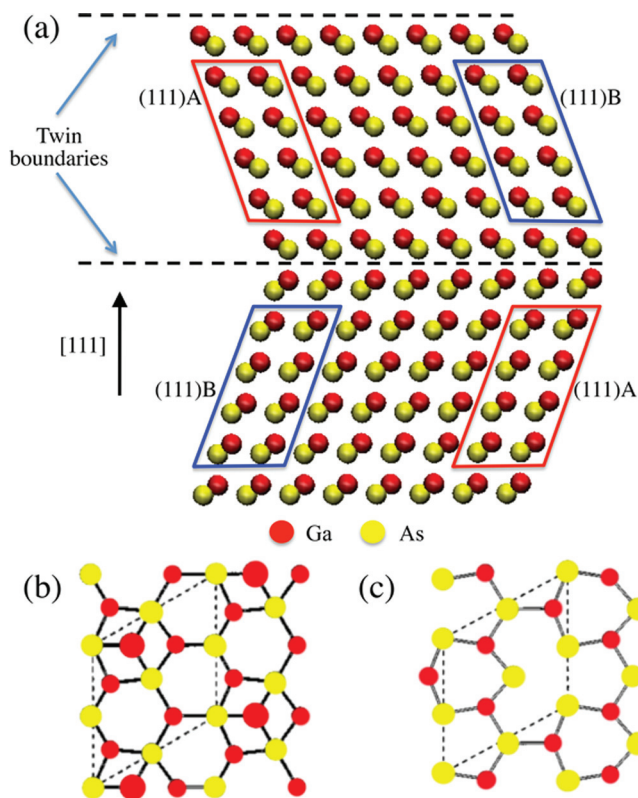


FIG. 1. Twinned GaAs nanosheet. (a) Relaxed GaAs crystal viewed from the  $[1\bar{1}2]$  direction, where red and yellow spheres represent Ga and As atoms, respectively. Atoms that belong to (111)A and (111)B regions are enclosed by red and blue lines, respectively. (b) Top view of the Ga-atom reconstruction of GaAs (111)B surface. (c) Top view of the Ga-vacancy reconstruction of (111)A surface.

GaAs (111)A sidewalls with Ga-vacancy reconstructions (Fig. 1(c)). These reconstructed surfaces are charge-neutral and have the lowest surface energies compared with other surfaces at most Ga and As vapor pressures.<sup>26</sup> The NS with these reconstructed sidewall surfaces remains stable during the quasi-Newton energy minimization.

**Surface electronic states:** We study the KS energy levels that lie in the bulk band gap. Since the effect of twin boundaries on the energy levels is known to be very small,<sup>8,9</sup> such gap states, if they exist, are expected to arise from the resulting alternating (111)A and (111)B sidewall surfaces. To quantify these surface states, we calculate the electronic partial density-of-states<sup>27</sup> (PDOS)  $D_{\alpha}(E)$  projected onto the wave functions of the atoms in the surface regions ( $\alpha = (111)A$  or (111)B). The definition of these surface regions is shown in Fig. 1(a). In Fig. 2(a), the red and blue curves show the calculated  $D_{(111)A}(E)$  and  $D_{(111)B}(E)$ , respectively, where the origin of the energy is the Fermi energy. To show the alignment of these surface energy levels relative to the band gap ( $\sim 1.5$  eV) of the bulk GaAs, bulk conduction-band (CB) and valence-band (VB) energies are marked by orange and green boxes, respectively, in Fig. 2(a). The gap states derived from (111)A surfaces are located just above the bulk VB top. On the other hand, those derived from (111)B surfaces are located just below the bulk CB bottom. These band alignments are illustrated in Fig. 2(b). To understand the nature of the band alignment, we project the CB-edge and VB-edge wave functions onto the pseudoatomic orbitals centered at Ga and As atoms.<sup>28</sup>

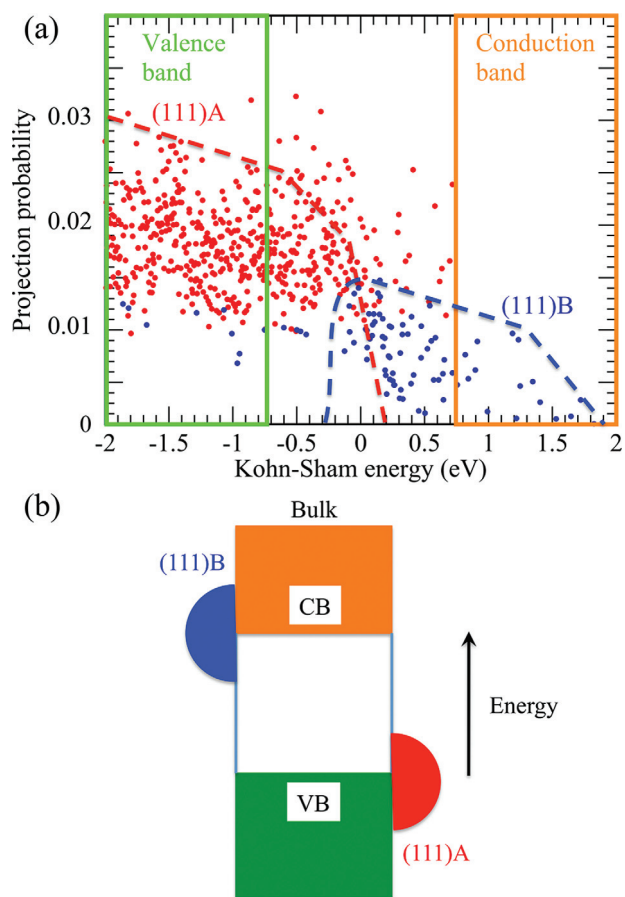


FIG. 2. Surface electronic states. (a) Electronic partial densities-of-states (PDOS) projected onto the (111)A and (111)B sidewall surfaces defined in Fig. 1(a) are shown by red and blue curves, respectively. Bulk conduction-band (CB) and valence-band (VB) energies are marked by orange and green boxes, respectively. (b) Schematic of the bulk CB (orange) and VB (green) along with (111)A (red) and (111)B (blue) surface-state energies.

For the CB-edge wave function, 67.6% and 32.4% of the total population come from Ga 4s and As 4s states, respectively.<sup>8</sup> The partial populations of the three degenerate VB-edge wave functions, on the other hand, are nearly identical: 80.3% and 11.6%, respectively, from As 4p and Ga 4p states.<sup>8</sup> Namely, the CB wave function is s-like and is centered at Ga atoms, whereas the VB wave functions are p-like around As atoms. The reconstructed (111)A surface is characterized by Ga vacancy sites, and hence, it is more As-like. Since the VB-edge wave functions reside dominantly on As atoms, it is understandable that the calculated PDOS of (111)A surfaces has a larger weight near the VB edge. On the contrary, the reconstructed (111)B surface has Ga adatoms, and hence is more Ga-like. Accordingly, its PDOS has more weight near the CB edge, where wave functions reside more on Ga atoms.

**Energy relaxation dynamics of photoexcited electron-hole pairs:** To study how the surface gap states affect CR, we perform nonadiabatic quantum molecular dynamics (NAQMD) simulations.<sup>27,29-32</sup> The NAQMD method describes electronic excitations in the framework of linear-response time-dependent density functional theory.<sup>33</sup> In addition, nonadiabatic transitions between excited electronic states assisted by molecular motions are treated with a surface-hopping approach.<sup>34-37</sup> To perform large NAQMD simulations involving many hundreds of atoms, we have

implemented a series of techniques for efficiently calculating the long-range exact exchange correction and excited-state forces.<sup>21,22</sup> Due to the use of excited-state forces, photoexcitation also modifies ground-state electronic structures.

To mimic photoexcitation in the bulk, we excite an electron from an occupied KS orbital with energy equal to the bulk VB top (Fig. 2(a)) to an unoccupied KS orbital with energy equal to the bulk CB bottom (Fig. 2(a)). In Fig. 3, the blue and red dots show the energy levels of the electron and hole states, respectively, as a function of time. Initially, only one electron-hole pair exists, where the difference between the electron and hole energies is  $\sim 1.5$  eV. Due to nonadiabatic transitions assisted by atomic motions, however, more electron-hole pairs are created starting at  $\sim 80$  fs concentrated near the Fermi energy.

To quantify the CR rate governed by the multiple excitations, we calculate the average electronic excitation energy

$$E_{\text{exc}}(t) = \frac{\sum_i n_i(t) \varepsilon_i(t) \Theta(\varepsilon_i(t)) - \sum_i (2 - n_i(t)) \varepsilon_i(t) \Theta(-\varepsilon_i(t))}{\sum_i n_i(t) \Theta(\varepsilon_i(t)) + \sum_i (2 - n_i(t)) \Theta(-\varepsilon_i(t))}, \quad (1)$$

where  $n_i(t)$  and  $\varepsilon_i(t)$  are the occupation number and energy of the  $i$ -th state at time  $t$ , and the step function  $\Theta(x)$  is 1 ( $x \geq 0$ ) or 0 ( $x < 0$ ). Figure 4 shows the calculated  $E_{\text{exc}}(t)$  in a semi-log plot. The linear decrease represented by the solid line in Fig. 4 indicates an exponential decay of the excitation energy,  $E_{\text{exc}}(t) = E_0 \exp(-k_{\text{CR}} t)$ , where  $E_0$  is the photo-excitation energy and  $k_{\text{CR}}$  is the CR rate. The best fit yields  $k_{\text{CR}} = (3.0 \pm 0.2) \times 10^{11} \text{ (s}^{-1}\text{)}$ . The corresponding decay time of a few ps is consistent with a value inferred for GaAs NWs from recent optical pump-terahertz probe measurements.<sup>10</sup>

*Surface recombination velocity:* The CR time  $\tau$  in NWs is commonly expressed as

$$\frac{1}{\tau} = \frac{1}{\tau_{\text{bulk}}} + \frac{4S}{d}, \quad (2)$$

where  $\tau_{\text{bulk}}$  is the bulk CR time,  $d$  is the NW diameter, and  $S$  is the SRV. Joyce *et al.* performed optical pump-terahertz probe experiments to measure the decay time of

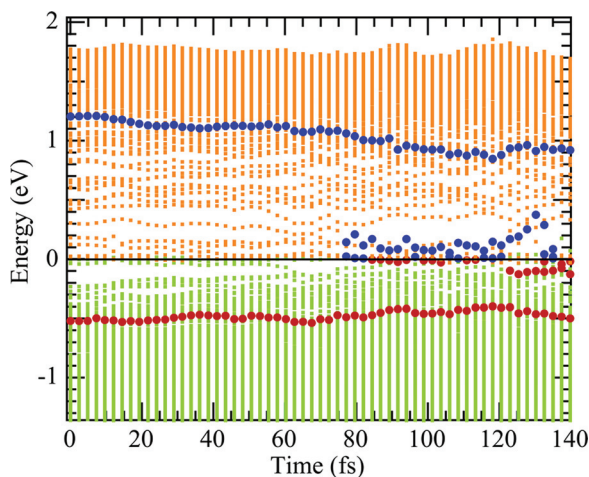


FIG. 3. Energy relaxation of photoexcited electron-hole pairs. Electron (solid blue circle) and hole (solid red circle) energy levels are shown as a function of time. The other occupied and unoccupied energy levels are shown by green and orange dots, respectively.

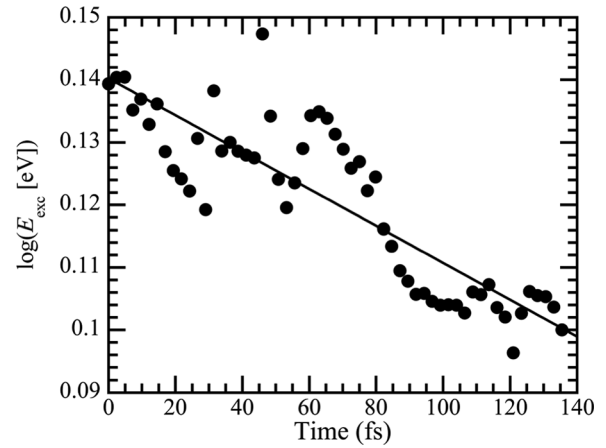


FIG. 4. The average electronic excitation energy as a function of time.

photoexcited carriers in GaAs NWs of diameter  $d = 30, 50,$  and  $80 \text{ nm}$ .<sup>10</sup> They fitted the measured diameter-dependent decay time to Eq. (2) and estimated  $S = 5.4 \times 10^3 \text{ m/s}$ .

To compare our NAQMD simulation results with these experiments, we construct a simple model as follows: Consider a cylindrical NW of diameter  $d$ , in which the CR rate is much larger than the bulk value in the outer shell of thickness  $\delta$  as shown in Fig. 5(a). An electron-hole pair photoexcited in the core of the NW must first diffuse to the shell to recombine at a rate of  $k_{\text{CR}}$ . We solve a simple diffusion-reaction equation for the photoexcited carrier population using the diffusion coefficient of  $D = 10^{-3} \text{ m}^2/\text{s}$  (a typical value for a hole in bulk GaAs). From the spatial decay of typical surface states observed in our simulation, we estimate  $\delta = 1 \text{ nm}$ . Figure 5(b) shows the calculated carrier population as a function of time for  $d = 30, 50,$  and  $80 \text{ nm}$ . We see more rapid decay of carriers for smaller  $d$ . From the exponential fit (solid lines in Fig. 5(b)), we obtain the effective CR rate for each diameter  $d$ . Figure 5(c) shows the fitted  $k_{\text{CR}}$  as a function of  $d$ . By fitting the result with Eq. (2), we obtain the SRV to be  $(3.6 \pm 0.9) \times 10^3 \text{ m/s}$ . This value is the same order-of-magnitude as the experimental value of  $5.4 \times 10^3 \text{ m/s}$ . Thus, the TSL and associated  $\{111\}$  sidewall surfaces can quantitatively account for the experimentally observed large SRV in GaAs NWs. It is also understandable that the calculated SRV is slightly smaller than the experimental value, since the former is for the ideal reconstructed surfaces and does not include the contributions of surface oxidation and other defects. Possible defects in experimental systems include vacancies and impurities (*e.g.*, carbon) introduced during the growth.

The high SRV of a twinned GaAs NW may be understood as a consequence of the unique electronic structures associated with its geometry. Namely, alternating (111)A and (111)B sidewall surfaces with, respectively, near VB-edge and CB-edge energies provide spatially proximate CR sites. Photoexcited electrons tend to migrate quickly to (111)B surfaces driven by the energy alignment, while holes migrate to (111)A surfaces. With a high density of twin defects (*i.e.*, short length scales of alternating (111)A and (111)B surface segments), the electron and hole wave functions have considerable overlap and hence a large CR rate and SRV. To confirm that the very large SRV is a

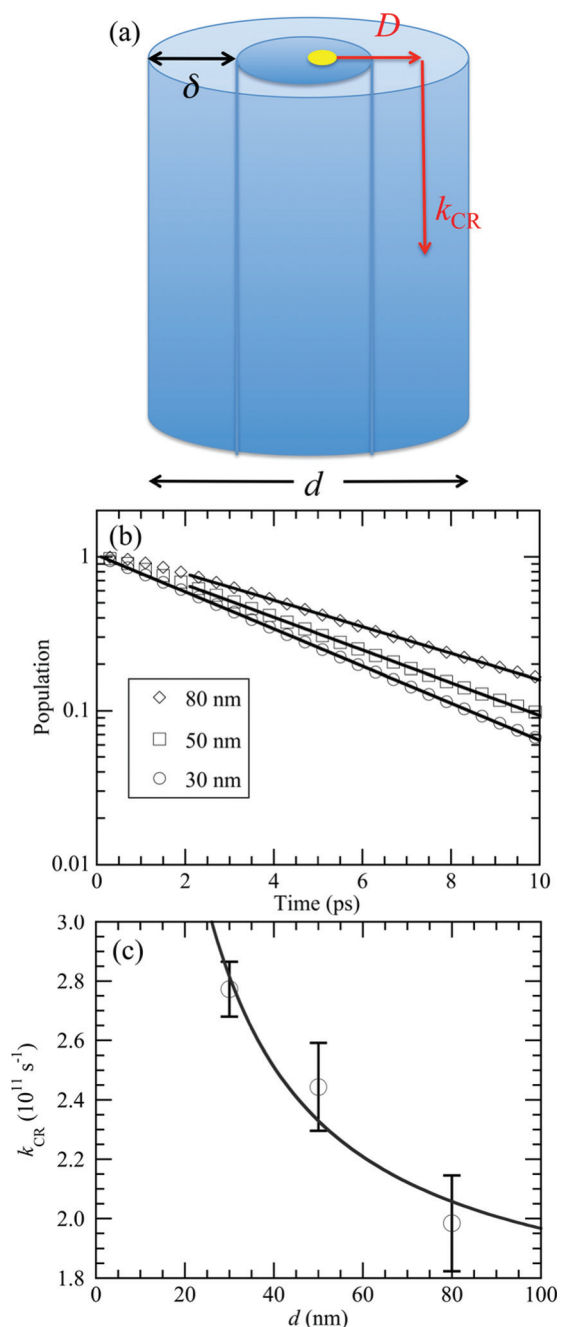


FIG. 5. (a) Schematic of carrier diffusion and charge recombination (CR) in a GaAs NW. (b) Carrier population as a function of time for diameter  $d = 30, 50,$  and  $80$  nm. (c) The CR rate as a function of the NW diameter.

consequence of the unique surface geometry associated with TSLs, we have performed another simulation, in which the sidewall surface is (110) instead of alternating (111)A/(111)B. The calculated CR rate at the (110) surface is orders-of-magnitude smaller ( $\sim 10^7 \text{ s}^{-1}$ ).<sup>38</sup> Hence, the much larger CR rate ( $\sim 10^{11} \text{ s}^{-1}$ ) in this paper is likely due to the TSL-related surface geometry.

In summary, our NAQMD simulations have shown that unique surface electronic states at alternating (111)A and (111)B sidewall surfaces of twinned GaAs NWs act as effective CR centers. The calculated SRV quantitatively explains recent experimental observations. Such atomistic understanding lays a foundation for the rational design of GaAs NW-based devices.

This work was supported by the U.S. Department of Energy, Office of Science, Office of Basic Energy Sciences under Award DE-SC0001013 as part of the Center for Energy Nanoscience, an Energy Frontier Research Center. Simulations were performed at the Center for High Performance Computing and Communications of the University of Southern California.

- <sup>1</sup>J. A. Czaban, D. A. Thompson, and R. R. LaPierre, *Nano Lett* **9**(1), 148 (2009).
- <sup>2</sup>J. Wallentin, N. Anttu, D. Asoli, M. Huffman, I. Aberg, M. H. Magnusson, G. Siefert, P. Fuss-Kailuweit, F. Dimroth, B. Witzigmann, H. Q. Xu, L. Samuelson, K. Deppert, and M. T. Borgstrom, *Science* **339**(6123), 1057 (2013).
- <sup>3</sup>G. Mariani, A. C. Scofield, C. H. Hung, and D. L. Huffaker, *Nat. Commun.* **4**, 1497 (2013).
- <sup>4</sup>M. Yao, N. Huang, S. Cong, C.-Y. Chi, M. A. Seyedi, Y.-T. Lin, Y. Cao, M. L. Povinelli, P. D. Dapkus, and C. Zhou, *Nano Lett.* **14**(6), 3293 (2014).
- <sup>5</sup>Q. H. Xiong, J. Wang, and P. C. Eklund, *Nano Lett.* **6**(12), 2736 (2006).
- <sup>6</sup>R. E. Algra, M. A. Verheijen, M. T. Borgstrom, L. F. Feiner, G. Immink, W. J. P. van Enkevort, E. Vlieg, and E. P. A. M. Bakkers, *Nature* **456**(7220), 369 (2008).
- <sup>7</sup>P. Caroff, K. A. Dick, J. Johansson, M. E. Messing, K. Deppert, and L. Samuelson, *Nat. Nanotechnol.* **4**(1), 50 (2009).
- <sup>8</sup>K. Shimamura, Z. Yuan, F. Shimojo, and A. Nakano, *Appl. Phys. Lett.* **103**(2), 022105 (2013).
- <sup>9</sup>Z. Yuan and A. Nakano, *Nano Lett.* **13**(10), 4925 (2013).
- <sup>10</sup>H. J. Joyce, C. J. Docherty, Q. Gao, H. H. Tan, C. Jagadish, J. Lloyd-Hughes, L. M. Herz, and M. B. Johnston, *Nanotechnology* **24**(21), 214006 (2013).
- <sup>11</sup>T. Watanabe, K. Tsumura, and I. Ohdomari, *Phys. Rev. Lett.* **96**(19), 196102 (2006).
- <sup>12</sup>S. Hirose, I. Yamashita, R. Nagumo, R. Miura, A. Suzuki, H. Tsuboi, N. Hatakeyama, A. Endou, H. Takaba, M. Kubo, and A. Miyamoto, *Jpn. J. Appl. Phys., Part 1* **50**(4), 04DP05 (2011).
- <sup>13</sup>F. Shimojo, S. Ohmura, R. K. Kalia, A. Nakano, and P. Vashishta, *Phys. Rev. Lett.* **104**(12), 126102 (2010).
- <sup>14</sup>K. Shimamura, F. Shimojo, R. K. Kalia, A. Nakano, and P. Vashishta, *Phys. Rev. Lett.* **111**(6), 066103 (2013).
- <sup>15</sup>K. Shimamura, F. Shimojo, R. K. Kalia, A. Nakano, K. Nomura, and P. Vashishta, *Nano Lett.* **14**(7), 4090 (2014).
- <sup>16</sup>P. Hohenberg and W. Kohn, *Phys. Rev.* **136**(3B), B864 (1964).
- <sup>17</sup>P. E. Blochl, *Phys. Rev. B* **50**(24), 17953 (1994).
- <sup>18</sup>G. Kresse and D. Joubert, *Phys. Rev. B* **59**(3), 1758 (1999).
- <sup>19</sup>J. P. Perdew, K. Burke, and M. Ernzerhof, *Phys. Rev. Lett.* **77**(18), 3865 (1996).
- <sup>20</sup>S. G. Louie, S. Froyen, and M. L. Cohen, *Phys. Rev. B* **26**(4), 1738 (1982).
- <sup>21</sup>F. Shimojo, S. Ohmura, W. Mou, R. K. Kalia, A. Nakano, and P. Vashishta, *Comput. Phys. Commun.* **184**(1), 1 (2013).
- <sup>22</sup>F. Shimojo, R. K. Kalia, M. Kunaseth, A. Nakano, K. Nomura, S. Ohmura, K. Shimamura, and P. Vashishta, *J. Chem. Phys.* **140**(18), 18A529 (2014).
- <sup>23</sup>J. Ihm, A. Zunger, and M. L. Cohen, *J. Phys. C: Solid State Phys.* **12**(21), 4409 (1979).
- <sup>24</sup>C.-Y. Chi, C.-C. Chang, S. Hu, T.-W. Yeh, S. B. Cronin, and P. D. Dapkus, *Nano Lett.* **13**(6), 2506 (2013).
- <sup>25</sup>Z. Yuan, K. Shimamura, F. Shimojo, and A. Nakano, *J. Appl. Phys.* **114**(7), 074316 (2013).
- <sup>26</sup>N. Moll, A. Kley, E. Pehlke, and M. Scheffler, *Phys. Rev. B* **54**(12), 8844 (1996).
- <sup>27</sup>W. Mou, S. Ohmura, F. Shimojo, and A. Nakano, *Appl. Phys. Lett.* **100**(20), 203306 (2012).
- <sup>28</sup>F. Shimojo, A. Nakano, R. K. Kalia, and P. Vashishta, *Phys. Rev. E* **77**(6), 066103 (2008).
- <sup>29</sup>C. F. Craig, W. R. Duncan, and O. V. Prezhdo, *Phys. Rev. Lett.* **95**(16), 163001 (2005).
- <sup>30</sup>C. P. Hu, H. Hirai, and O. Sugino, *J. Chem. Phys.* **127**(6), 064103 (2007).
- <sup>31</sup>E. Tapavicza, I. Tavernelli, and U. Rothlisberger, *Phys. Rev. Lett.* **98**(2), 023001 (2007).

- <sup>32</sup>X. Zhang, Z. Li, and G. Lu, *Phys. Rev. B* **84**(23), 235208 (2011).
- <sup>33</sup>M. E. Casida, in *Recent Advances in Density Functional Methods (Part I)*, edited by D. P. Chong (World Scientific, Singapore, 1995), pp. 155–192.
- <sup>34</sup>J. C. Tully, *J. Chem. Phys.* **93**(2), 1061 (1990).
- <sup>35</sup>J. R. Schmidt, P. V. Parandekar, and J. C. Tully, *J. Chem. Phys.* **129**(4), 044104 (2008).
- <sup>36</sup>O. V. Prezhdo, *J. Chem. Phys.* **111**(18), 8366 (1999).
- <sup>37</sup>A. W. Jasper, S. N. Stechmann, and D. G. Truhlar, *J. Chem. Phys.* **116**(13), 5424 (2002).
- <sup>38</sup>E. Brown, C. Sheng, F. Shimojo, and A. Nakano, “Enhanced charge recombination due to surfaces and twin defects in GaAs nanostructures” (unpublished).